# Direct Formation of Reduced Graphene Oxide and 3D Lightweight Nickel Network Composite Foam by Hydrohalic Acids and Its Application for High-Performance Supercapacitors

Haifu Huang, Yanmei Tang, Lianqiang Xu, Shaolong Tang,* and Youwei Du

Jiangsu Key Laboratory for Nanotechnology, Nanjing National Laboratory of Microstructures and Department of Physics, Nanjing University, Nanjing 210093, People's Republic of China

Ⓢ Supporting Information

**ABSTRACT:** Here, a novel graphene composite foam with 3D lightweight continuous and interconnected nickel network was successfully synthesized by hydroiodic (HI) acid using nickel foam as substrate template. The graphene had closely coated on the backbone of the 3D nickel conductive network to form nickel network supported composite foam without any polymeric binder during the HI reduction of GO process, and the nickel conductive network can be maintained even in only a small amount of nickel with 1.1 mg/cm$^2$ and had replaced the traditional current collector nickel foam (35 mg/cm$^2$). In the electrochemical measurement, a supercapacitor device based on the 3D nickel network and graphene composite foam exhibited high rate capability of 100 F/g at 0.5 A/g and 86.7 F/g at 62.5 A/g, good cycle stability with capacitance retention of 95% after 2000 cycles, low internal resistance (1.68 Ω), and excellent flexible properties. Furthermore, the gravimetric capacitance (calculated using the total mass of the electrode) was high up to 40.9 F/g. Our work not only demonstrates high-quality graphene/nickel composite foam, but also provides a universal route for the rational design of high performance of supercapacitors.

**KEYWORDS:** supercapacitor, graphene foam, 3D network, nickel foam, current collector
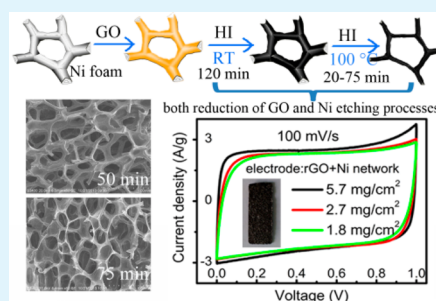


## 1. INTRODUCTION

Supercapacitors as ideal energy storage devices have attracted intense interest, due to their outstanding electrochemical performance such as high power density, fast charging–discharging rate, and excellent cycle stability.[1−4] On the basis of the mechanism of energy storage, supercapacitors can be categorized into two forms: electrochemical double-layer capacitors (EDLCs), which store energy from the reversible adsorption/desorption of ion at the interface between the electrode and the electrolyte, and pseudocapacitors, which store energy from rapid surface redox reactions in the electrode material with the electrolyte. The EDLCs are mainly fabricated from carbon materials, including activated carbons, carbon nanotubes, and graphene. For pseudocapacitors, electrode materials mainly include metal oxides/hydroxides[5] and conducting polymers.[6−10] Pseudocapacitors exhibit high capacitance but relatively poor cyclic stability, which limited their application. On the contrast, EDLCs have higher power density and better electrochemical cyclic stability than pseudocapacitors, but their energy densities are often low. Despite this, the electrodes used in most commercial supercapacitors are made of inexpensive and corrosion-resistant carbon materials currently. Among various types of electrode materials for EDLCs, graphene-based material has gained more interest due to their superior electrical conductivity, exceptionally high surface area, and excellent mechanical flexibility, and

has shown excellent power density and life-cycle stability.[11−18] Especially, reduced graphene oxide (rGO) can be obtained by reduction of graphene oxide (GO) cost-effectively on a large scale, leading to an attractive application prospect for energy storage and conversion. In addition, graphene as an ideal platform is easy to use to build graphene-based composites with metal oxides, and conducting polymers for supercapacitor applications.[19] Also, methods for synthesis of graphene have been developed such as the cross-linking method,[20] hydrothermal method,[21,22] and chemical vapor deposition (CVD) growth on metal substrates.[23−26] Nowadays, various graphene-based materials have been successfully prepared and show a high specific capacitance as supercapacitors.[21,27−32]

However, as supercapacitor electrode materials, only a few high conductive graphenes film or foam can be directly used as electrode without additional current collector, such as a porous reduced graphene oxide ultrathin film produced via unique laser reduction approach showed excellent conductivity (1738 S/m),[33] and ultrathin-graphite foam can be replaced by traditional current collectors such as nickel foam or carbon paper.[34] However, there are some disadvantages for them: overall or areal specific capacitance of graphene oxide ultrathin film is too
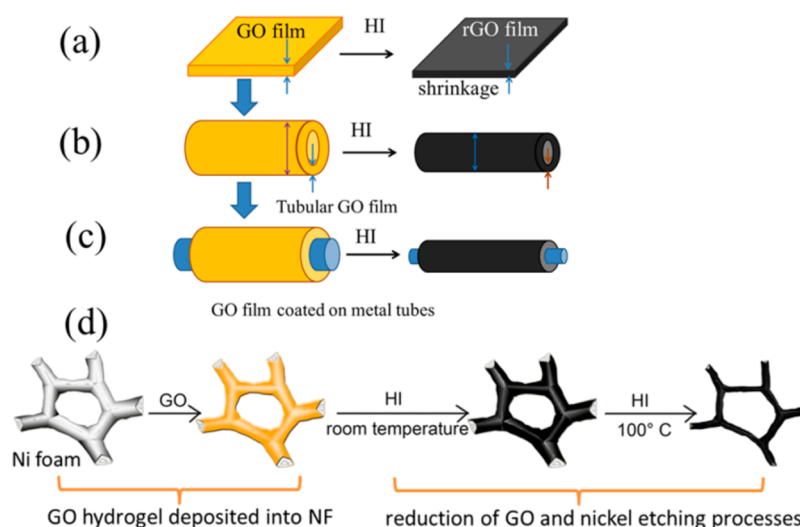
**Figure 1.** (a) Schematic illustration of HI acid-reduced graphene film shrinkage. (b) HI reduction simulation of a tubular GO film. (c) HI reduction simulation of GO film coated on micrometer metal tubes. (d) Schematic illustration of the rGO@Ni electrode preparation process.

low to be used for practical applications due to a low mass loading of graphene ultrathin film; and ultrathin-graphite foam has limited its practical application on a large scale because of the low-yield production and high production costs of CVD method. In most cases, many macroporous rGO films or free-standing 3D graphene foam still need to be attached on the metal foils or metal conductive film when assembled into electrode, let along the graphene powder. It will lead to a very low gravimetric specific capacitance of total electrode (calculated using the total mass of the electrode), because the current collector often makes up most of the total mass of electrode in a lot of cases. For example, 3D graphene aerogel on nickel foam reported by Feng et al. shows a high specific capacitance of 366 F/g at a current density of 2 A/g,[28] but considering the weight of Ni foam (the typical density of nickel foam is about ~35 mg/cm$^2$, and the mass of rGO is about ~1 mg/cm$^2$), the gravimetric specific capacitance of 3D graphene aerogel on nickel foam would be low to ~8 F/g. Furthermore, it would increase higher contact resistance between graphene material and the current collector, resulting in bad performance such as low rate capability and poor cycle stability, as even the graphene-based materials possess high electrical conductivity and large surface area. The total mass of the electrode and contact resistance between graphene material and the current collector must be taken into consideration in practical applications.[34,35] Therefore, it is still a challenge to meet these criteria including high gravimetric specific capacitance of total electrode, high rate capability, and low production costs in practical application of supercapacitor. To achieve this goal, the electrode material and current collector should be integrated together in depth rather than that electrode material is simply attached on the current collector by binder, and a 3D lightweight metal conductive network should replace the traditional current collector such as metal foam, metal foil, and metal films to reduce the total mass of the electrode.

In this work, by taking advantage of shrinkage of HI acid-reduced graphene film thickness and anticorrosive effect of graphene for metal, a 3D lightweight conductive network was cleverly embedded into the inside of graphene foam using commercial nickel foam as substrate template during the process of reduction of GO and nickel etching. After both reduction of GO and nickel etching processes in HI solution,

3D nickel conductive backbone was maintained perfectly even in only a small amount of nickel with 1.1 mg/cm$^2$. In other words, Ni foam with 30 mg/cm$^2$ as current collector was replaced by lightweight nickel conductive network (1.1 mg/cm$^2$), which greatly reduces the total mass of the electrode. To our knowledge, there are few reports about the integration of graphene foam into lightweight metal conductive network as electrode materials. In the electrochemical measurement, the flexible supercapacitor device based on 3D Ni network and graphene composite foam (labeled as rGO@Ni), which did not need any additional metal current collector, displays remarkable high rate capability performance and excellent flexible property.

## 2. EXPERIMENTAL SECTION

**2.1. Preparation of rGO@Ni Electrode.** Graphite oxide (GO) was prepared by a modified Hummers' method. Ni foam (110 PPI, mass density of ~30 mg/cm$^2$, Shanxi Lizhiyuan Battery Material Co., Ltd., China) was carefully cleaned and treated with acetone and hydrochloric acid to remove contaminants, and then washed in sequence with deionized water and absolute ethanol. The synthesis of rGO@Ni is illustrated in Figure 1d. In brief, a cleaned nickel foam sheet (with a size of $2.5 \times 1.0 \times 0.1$ cm) was put into a centrifugal tube containing GO dispersions (4 mg/mL), then centrifuged at 50 rpm to fill GO hydrogel into the micropores and coat the network of the wet nickel foam. After 15 min, the nickel foam was taken out, and dried for several hours to remove the water at room temperature. This process was repeated for a number of times to increase the GO loading. After that, a nickel foam sheet coated with GO had been immersed into HI aqueous solution (45%) for 120 min at room temperature and then maintained at 100 °C in an oil bath for about 1 h, washed with a large amount of distilled water and ethanol, and finally dried for 12 h at room temperature to remove the water.

For comparison, the rGO foam with nickel all etched was prepared in a procedure similar to that of rGO@Ni. Briefly, a nickel foam sheet coated with GO had been immersed into HI aqueous solution (45%) for 120 min at room temperature and then maintained at 100 °C in an oil bath for about 10 h to completely dissolve the nickel foam. The rGO foam was pressed into Ti foil for electrochemical measurement.

To measure the mass of rGO, rGO@Ni sheet was put into 6 M HCl acid at 80 °C for 6 h to completely remove the Ni and then rinsed gently with a large amount of deionized water and ethanol and finally dried under ambient conditions at 60 °C.

**2.2. Electrochemical Measurement.** A two-electrode cell configuration was used to measure the performance of rGO@Ni as
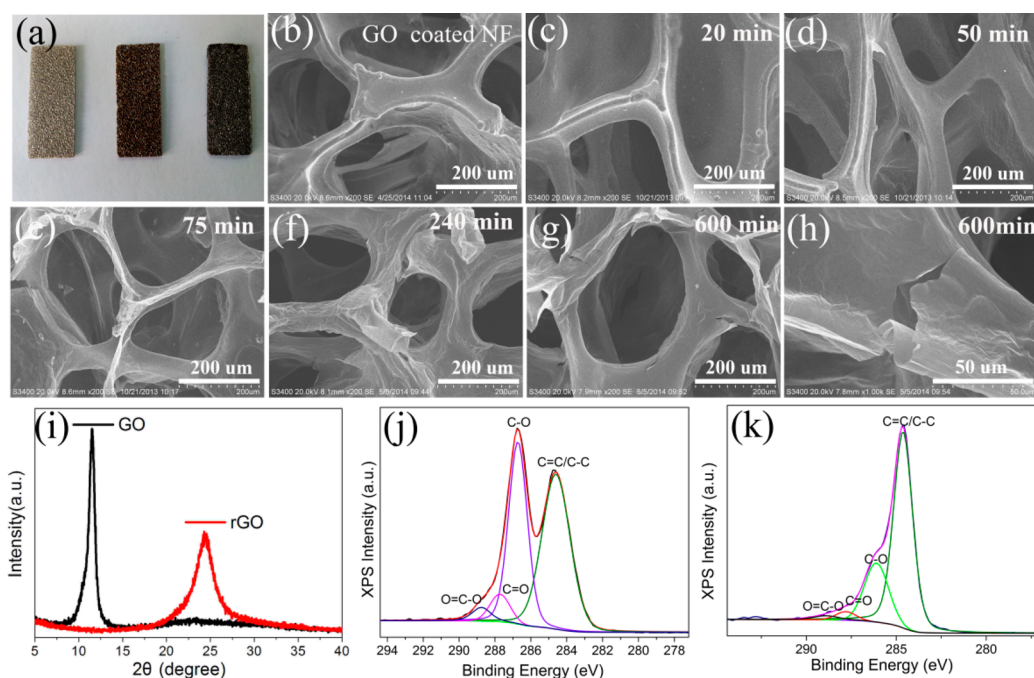
**Figure 2.** (a) Digital photographs of nickel foam, GO gel coated on nickel foam, and rGO@Ni. SEM images at different magnifications: (b) GO coated Ni foam, as-prepared rGO@Ni maintained at 100 °C for 20 min (c), for 50 min (d), for 75 min (e), for 240 min (f), for 600 min (g), and for 600 min (h), respectively. (i) XRD patterns of GO and rGO foam. (j) The C 1s XPS spectra for GO and (k) for rGO foam.

a supercapacitor electrode. Two identical rGO@Ni electrodes (1.0 × 1.0 cm each) were separated by a thick separator (NKK TF45, 40 μm). A flexible supercapacitor device was assembled to measure the actual performances. As shown in Figure 6a, two pieces of flexible rGO@Ni (1.0 × 1.0 cm each) electrode attached on the PET membrane (∼30 μm) were assembled with a separator (NKK TF45, 40 μm) sandwiched between. All electrodes are without any binder or conduct additive. The electrochemical performances were characterized by cyclic voltammetry (CV), galvanostatic charge–discharge (GCD) tests, and electrochemical impedance spectroscopy (EIS) measurements in a 6 mol/L KOH aqueous solution.

The gravimetric specific capacitance was obtained from the discharge process according to the following equation:

$$C_s = 4I/(m\ dV/dt)$$

where $I$ is the applied current (A), $m$ is the total graphene mass of the two electrodes (g), and $dV/dt$ is the slope of the discharge curve (V/s).

The areal specific capacitance was obtained from the discharge process according to the following equation:

$$C_{areal} = 2I/(S\ dV/dt)$$

where $I$ is the applied current density (A), $S$ is the areal of the electrode (cm²), and $dV/dt$ is the slope of the discharge curve (V/s).

The energy density ($E$) and power density ($P$) of a supercapacitor device in the Ragone plots were calculated using the following equations:

$$E = C_s\Delta V^2/8$$

$$P = E/\Delta t$$

$\Delta V$ is the sweep potential window, and $\Delta t$ is the discharge time.

**2.3. Material Characterization.** The morphology of rGO foam was examined using a scanning electron microscope (SEM, Hi-tachi S3400, Japan). X-ray diffraction (XRD) patterns were performed on X-ray diffraction (X'TRA, Thermo ARL X'TRA, Switzerland) with Cu Kα radiation in the range of 5−40°. X-ray photoelectron spectroscopy (XPS) was carried out using Phi 5000 VersaProbe Scanning ESCA Microprobe (Ulvac-Phi, Inc., Japan). Raman spectra were recorded on

a Raman spectrometer (LabRAM HR, Horiba Jobin Yvon Inc., France) using 632.8 nm wavelength laser. Electrochemical performance measurements were carried out using an electrochemical workstation (CHI 660D, Chenhua Instruments, China).

## 3. RESULTS AND DISCUSSION

**3.1. Synthetic Mechanism, Morphology, and Chemical Structure.** Among a variety of chemical reducing agents such as hydrazine, hydrohalic acids, NaBH, alcohols, vitamin C, urea, and glutathione, only HI is very suitable for the reduction of GO films. Particularly, HI acid-reduced graphene film shows interesting shrinkage of the film thickness during the reduction process reported by Cheng[36] (demonstration in Figure 1a). Inspired by this phenomenon, if a tubular GO film replaces GO film in this reduction process, not only should it show the shrinkage of tube wall, but also its diameter may be decreased via reduction of HI (demonstration as shown in Figure 1b). Further, both reduction of GO film and metal etching processes could be carried out simultaneously when GO film is coated on micrometer metal tubes as shown in Figure 1c. Because of shrinkage of the rGO film and the blocking effect caused by graphene covered on metallic surfaces, the corrosion of which occurs in the cracks of graphene,[37] it is possible to obtain a composite structure of graphene coated with metal nanowires by control of reduction time. On the basis of these considerations, we choose commercial nickel foam as 3D substrate template to prepare 3D lightweight Ni network and graphene composite foam.

The novel 3D lightweight Ni network and graphene composite foam are designed on the basis of the following two key considerations. The first is to deposit GO gel into the micropores and tightly coat network of nickel foam. A nickel foam sheet was wetted fully by deionized water, and the color of Ni foam coated with GO gel became dark yellow as shown in Figure 2a. This process was repeated at least twice to induce more GO hydrogel attached to the surface of the network to
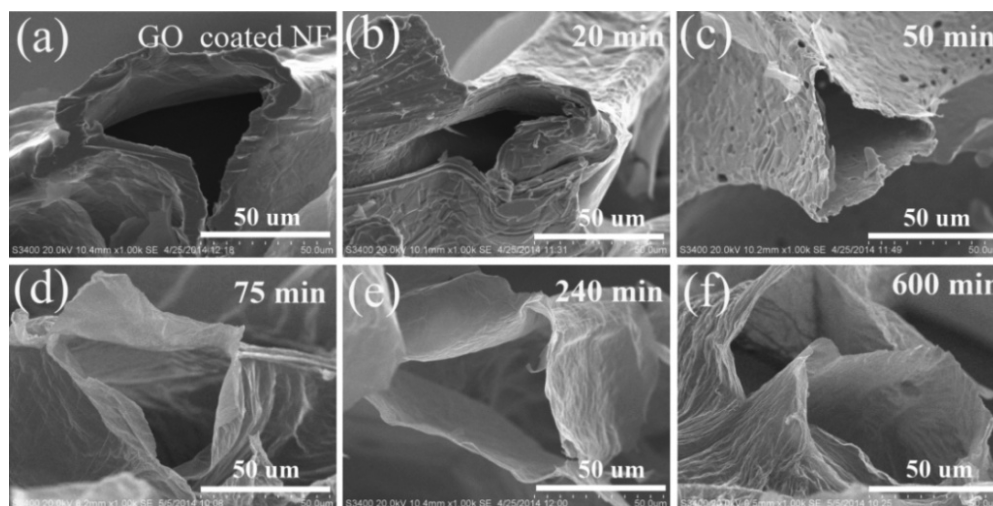
**Figure 3.** Cross-sectional SEM images: (a) GO coated Ni foam, rGO@Ni maintained at 100 °C for 20 min (b), for 50 min (c), for 75 min (d), for 240 min (e), and for 600 min (f), respectively. To obtain a cross-section, samples in (a) and (b) were cut by a sharp knife; and for (c), (d), (e), and (f), samples were torn in two parts.

increase the GO loading to prevent the graphene foam from collapsing and breaking without the support of Ni backbone during nickel etching due to the weakness of the thin graphitic wall.[26,38] Second, for the purpose that GO gel can be reduced effectively without breaking off and conductive backbone of nickel foam was maintained perfectly during nickel etching processes, Ni foam coated with GO gel was fully wetted by ethanol, which is better for making HI aqueous solution to penetrate into the micropores, then immersed into HI aqueous solution (45%) for 120 min, followed by maintaining at 100 °C in an oil bath for between 20 and 75 min. It is noteworthy that both reduction of GO and Ni etching processes are carried out simultaneously. The color of the GO gel became dark as shown in Figure 2a, and SEM images of samples maintained at 100 °C in an oil bath for 20, 50, and 75 min (shown in Figure 2c–e, respectively) show that the surface morphology has become wrinkled as the reduction process progressed, indicating GO has been effectively reduced by HI acid. At the same time, the SEM images also clearly show that a continuous and interconnected 3D network similar to Ni foam was obtained in the 3D graphene and Ni network composite foam, which facilitate the efficient access of electrolyte ions to the graphene surface and shorten the ion diffusion path.[12,39] It is noteworthy that shrinkage of the rGO skeleton occurs clearly as shown as in Figure 2d and e, and nickel conductive backbone was still interconnected by multimeter test (shown in Figure S1 and a video, Support Information), and Figure 2e shows the diameter becomes smaller, which is in agreement with our expectation. Further, Figure 2f–h and cross-sectional SEM images in Figure 3e and f show that rGO@Ni sample maintained at 100 °C for 240 and 600 min had been etched with Ni completely as compared to the cross-sectional SEM image of GO coated Ni foam (Figure 3a), but still kept a continuous and interconnected 3D network structure similar to that of Ni foam.

The structure and elemental characterization of rGO foam were further confirmed by XRD patterns and XPS spectra as given in Figure 2i–k. Figure 2i shows the XRD patterns of pristine GO and rGO. It is clear that the XRD pattern of GO shows a sharp peak indexed to (002) at 11.2°, corresponding to an interlayer spacing (d-spacing) of 0.772 nm. However, the peak at 11.2° has entirely disappeared after the GO is reduced

to rGO, and a broad diffraction peak is located at 24.1° with an interlayer space of 0.368 nm, due to the removal of the oxygen-containing groups from GO layers. Figure 2j and k shows the C 1s XPS spectra of GO and rGO foam. From the C 1s XPS spectrum of GO (Figure 2j), it shows two separated peaks consisting of two main components arising from C–O (hydroxyl and epoxy, 286.7 eV) and C=C/C–C (284.6 eV) species and two minor components from C=O (carbonyl, 287.7 eV) and O–C=O (carboxyl, 288.8 eV) species. In contrast, the C 1s XPS spectrum of rGO (Figure 2k) shows one single peak with a small tail in the higher binding energy region, the C=C/C–C bonds become dominant, and the hydroxyl and epoxy species of C–O and C=O reduced significantly, indicating that GO has been effectively reduced by HI acid.

The Raman spectra can be further used for examining the ordered and disordered crystal structures of reduced grapheme oxide. Generally, the $I_D/I_G$ intensity ratio was used to estimate the degree of disorder and average size of the sp$^2$ domains. As shown in Figure S2 (Supporting Information), there were two prominent peaks at 1329 and 1592 cm$^{-1}$ for GO, corresponding to the well-documented G and D bands, respectively. After the HI acid reduction, the intensity of D band (at 1323 cm$^{-1}$) is obviously increased, the G band shifts to 1585 cm$^{-1}$, and the $I_D/I_G$ intensity ratios increased obviously from 1.12 to 1.42, implying the existence of more defects/disorders in the graphene sheet. This phenomenon is similar to previous reports in the literature about the reduction of GO film by HI acid solution.[36]

During the reduction of GO and nickel etching processes, rGO wraps the backbone of Ni foam tightly and the conductive backbone of nickel foam was maintained perfectly even though the mass of nickel foam is only 1.1 mg/cm$^2$ after etching. Such a preparation method of nickel network supported graphene foam is better than that previously reported by us in that the mass of nickel conductive network is at least 5 mg/cm$^2$ after etching by HCl.[40] The synthetic mechanism of Ni network and graphene composite foam can be explained reasonably as follows. HI is very suitable for the reduction of GO films to equip them with high flexibility that can be applied on flexible devices.[36] The thickness of rGO film reduced by HI shows significant shrinkage, which leads to the structure being more
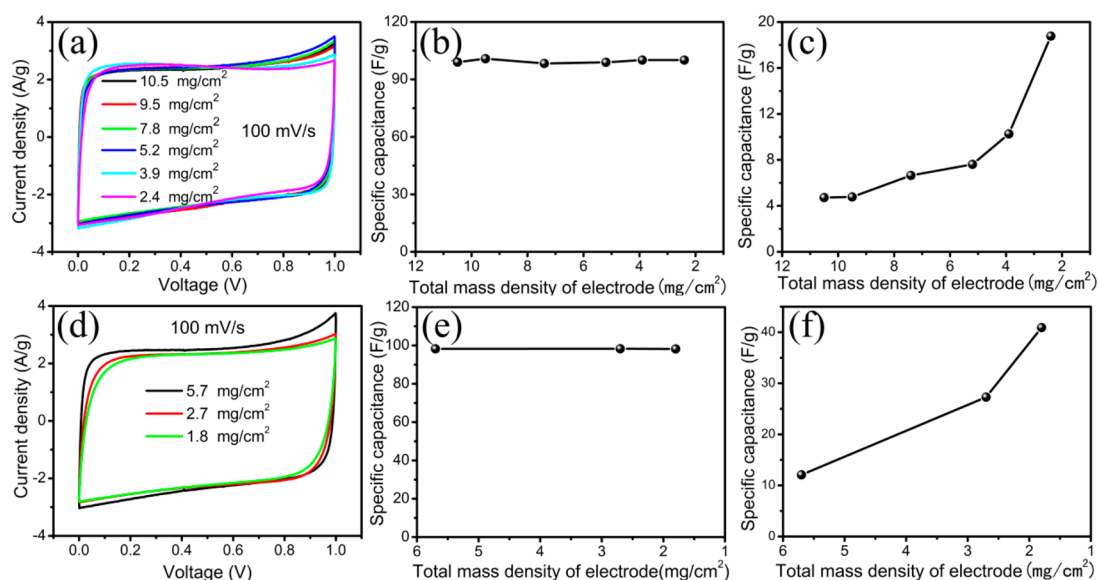
**Figure 4.** Different mass densities of rGO@Ni electrodes and the mass loading of rGO foam with 0.5, 0.45, 0.5, 0.4, 0.4, and 0.5 mg/cm$^2$, respectively: (a) CV curves at scan rate of 100 mV/s for different mass density of electrodes, (b) gravimetric specific capacitance calculated using the mass of rGO foam, and (c) gravimetric specific capacitance calculated using the total mass of electrode, respectively. rGO@Ni electrodes with the mass loading of rGO foam (0.7, 0.75, and 0.75 mg/cm$^2$, respectively.): (d) CV curves at scan rate of 100 mV/s, (e) gravimetric specific capacitance calculated using the mass of rGO foam, and (f) gravimetric specific capacitance calculated using the total mass of electrode, respectively.

compact. Therefore, the process in that Ni foam coated with GO gel was immersed into HI aqueous solution for 120 min at room temperature is favorable to rGO film adhering to the surface of the nickel foam and wrapping the backbone of Ni foam tightly, and nickel metal exposed to HI acid solution corroded slowly at this time. When the temperature rises to 100 °C, nickel metal exposed to HI acid solution is corroded rapidly, but higher temperature can make the reduction of GO films more effective.[36] Film thickness shrinks and backbone is wrapped more tightly, leading to the nickel metal surface coated with rGO film being harder to corrode because of the blocking effect caused by rGO,[37] thus resulting in that the diameter of rGO and Ni composite backbone become smaller with the increase of reduction time. These processes including both reduction of GO and nickel etching were reflected by SEM images and cross-sectional SEM images of samples as shown in Figures 2 and 3, respectively. Although nickel metal is corroded constantly, the conductive backbone of nickel foam can be still maintained due to a shrinkage of the film thickness tgat always exists and impels rGO film to wrap backbone tightly during both reduction of GO and nickel etching processes. During the HI treatment process, Ni support also may be completely removed at some locations, or its tubular structure has collapsed, which is wrapped with graphene, but it has no influence on the conductivity of the Ni network because the nickel skeleton is continuous and cross-linked together.

The rGO foam also maintains a Ni network obtained by etching away some Ni foam template by a simple etch treatment such as HCl, FeCl$_3$, and HNO$_3$ after reduction of GO, but bonding of rGO foam and Ni network is weaker than that of rGO@Ni with shrinkage of rGO films by the HI treatment, and thus it results in a bad contact, which is confirmed by comparing with our previously report.[40] Therefore, shrinkage of rGO films plays an important role in forming the 3D graphene and Ni network composite foam.

To further explore how much residual nickel metal is needed to keep the complete conductive network, we could simply

judge the conductive network as broken or not by multimeter using continuity testing with diode (buzzer) function (as shown in Figure S1 and a demo video, Supporting Information), and the mass of residual nickel network was measured by total mass of electrode minus mass of rGO. Table S1 (Supporting Information) shows the mass of residual nickel with complete conductive network from 3.4 to 1.1 mg/cm$^2$, and Table S2 (Supporting Information) shows the mass of residual nickel network, which had been destroyed from 1.4 to 0.4 mg/cm$^2$. Therefore, the mass of residual nickels is not less than 1.4 mg/cm$^2$ to ensure the complete conductive network can be maintained. In addition, time of oil bath maintained at 100 °C is better not more than 70 min according to our experimental results.

It is well-known that similar graphene foam prepared by CVD method using nickel foam template shows more high conductivity than that using chemical reduction due to the absence of defects and intersheet junction contact resistance; even this can be directly used as electrode without any metal current collectors, which not only eliminates the additional contact resistance between the current collector and the active material, but also reduces the total mass of the electrode.[26,34,38] Yet the low-yield production, high-quality CVD equipment, complex procedures, and high maintenance costs greatly limited its practical application on a large scale. Although chemically derived reduced graphene oxide is inherently less conductive than CVD-grown graphene, our approach could effectively improve the conductivity of chemical reduction graphene by embedding a lightweight conductive network rather than nickel foam into graphene foam inside cleverly. As compared to the CVD method, our approach is more cost-effective and can be applied to industrial levels on a large scale. Considering the cost and complexity of production process, the lightweight nickel network supported graphene foam can replace CVD-grown graphene to some extent.

**3.2. Electrochemical Performance.** To show our advantages of this novel design for real applications, we carried
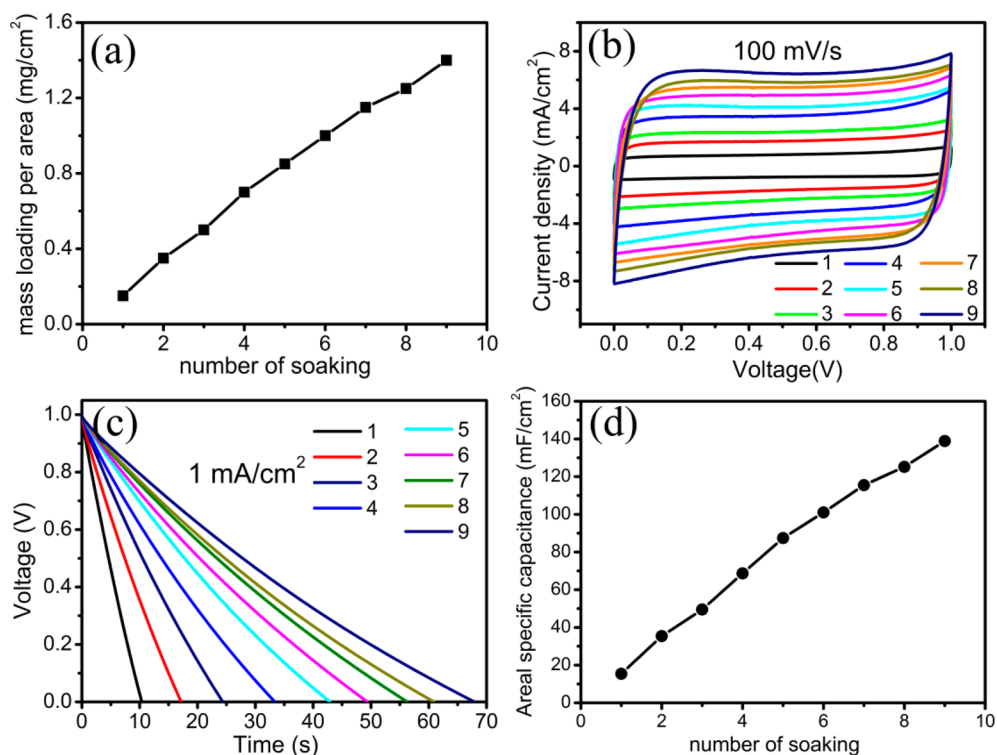
**Figure 5.** (a) The mass loading of rGO with number of soaking varied from 1 to 9. (b) CV curves at scan rates of 100 mV/s of rGO@Ni with number of soaking varied from 1 to 9. (c) Discharge curves at current density of 1 mA/cm^{2} with number of soaking varued from 1 to 9. (d) The areal specific capacitance of rGO@Ni with varied number of soaking.

out a detailed study using different mass densities of electrodes obtained with the etching time varying from 40 to 70 min to evaluate the influence of nickel network on the capacitance of the graphene foam composite electrodes. Cyclic voltammetry (CV) and galvanostatic charge−discharge (GCD) tests were carried out using a symmetric two-electrode configuration in a 6 mol/L KOH aqueous solution.[41] For a better comparison, all electrodes contain the same mass loading of rGO as far as possible. Figure 4a shows that there are no obvious differences of CV curves at scan rate of 100 mV/s for different mass densities of electrodes (mass density of electrodes: 10.5, 9.5, 7.8, 5.2, 3.9, and 2.4 mg/cm^{2}, corresponding to the mass loading of rGO of 0.5, 0.45, 0.5, 0.4, 0.4, and 0.5 mg/cm^{2}, respectively). Although the total mass of electrode has been gradually reduced by nickel etching, the specific capacitance is almost constant with a value of about 100 F/g calculated using mass of rGO as shown in Figure 4b (estimated from the discharging curves), indicating it is not necessary to retain the excess mass of nickel foam as long as a complete Ni conductive network of electrode can be maintained. To better illustrate the advantage of our approach, the gravimetric capacitance calculated using the total mass of the electrode with 2.4 mg/cm^{2} is ∼18.8 F/g and 4 times that for electrode of 10.5 mg/cm^{2} with a value of ∼4.7 F/g as shown in Figure 4c. With the increase in mass loading of the rGO, CV curves at scan rate of 100 mV/s (electrodes with 5.7, 2.7, and 1.8 mg/cm^{2}, corresponding to the mass loading of rGO for 0.7, 0.75, and 0.75 mg/cm^{2}, respectively) are almost consistent, but there was a slight change of the specific capacitance as shown in Figure 4d and e. However, the gravimetric capacitance is high up to 40.9 F/g calculated using the total mass of the electrode with 1.8 mg/cm^{2} as shown in Figure 4f, which is far higher than a freestanding three-dimensional graphene by atmospheric

pressure chemical vapor deposition (4.7 F/g, calculated for the entire electrode).[42] Moreover, Ni conductive network of the electrode with 1.8 mg/cm^{2} is only about 1 mg/cm^{2} and had been destroyed, but its CV curve is still close to typical quasi-rectangular shape at a scan rate of 100 mV/s. This study clearly illustrates that this novel design has a lot of advantages.

In addition, the difference of Ni support mass has some influence on the rate capability by comparison of CV scan rate, and charge−discharge rate, which are clearly shown in Figure S3 (Supporting Information). For example, as shown in Supporting Information Figure S3a and S3e, the CV curves of rGO@Ni with 5.4 and 1.9 mg/cm^{2} of nickel mass begin to deviate from the quasi-rectangular shape under scan rates of 8 and 1.5 V/s, respectively; however, the CV curves of rGO foam with nickel all etched deviated from the quasi-rectangular shape when the scan rate was just up to 0.4 V/s as shown in Supporting Information Figure S3i. Figure S3 (Supporting Information) clearly shows that the rGO foam without the support of the conductive network exhibits a worse performance than rGO@Ni electrodes by comparison of CV curves shape and IR drop of GCD curves of rGO@Ni with 5.4 and 1.9 mg/cm^{2} of nickel mass. The result was also confirmed by our previous study[40] and another report.[27] The influence of Ni support mass for electrochemical performance was further confirmed by the gravimetric specific capacitance values at different current densities and the electrochemical impedance spectroscopy (EIS) measured at open-circuit potential shown in Figures S4 and S5 (Supporting Information), respectively. Figure S4 (Supporting Information) clearly shows that the higher is the mass loading of Ni, the better is the rate capability of rGO. The equivalent series resistance (ESR) obtained from the Nyquist plot (Figure S5, Supporting Information) was about 0.51 and 1.38 Ω for rGO@Ni with 5.4 and 1.9 mg/cm^{2}
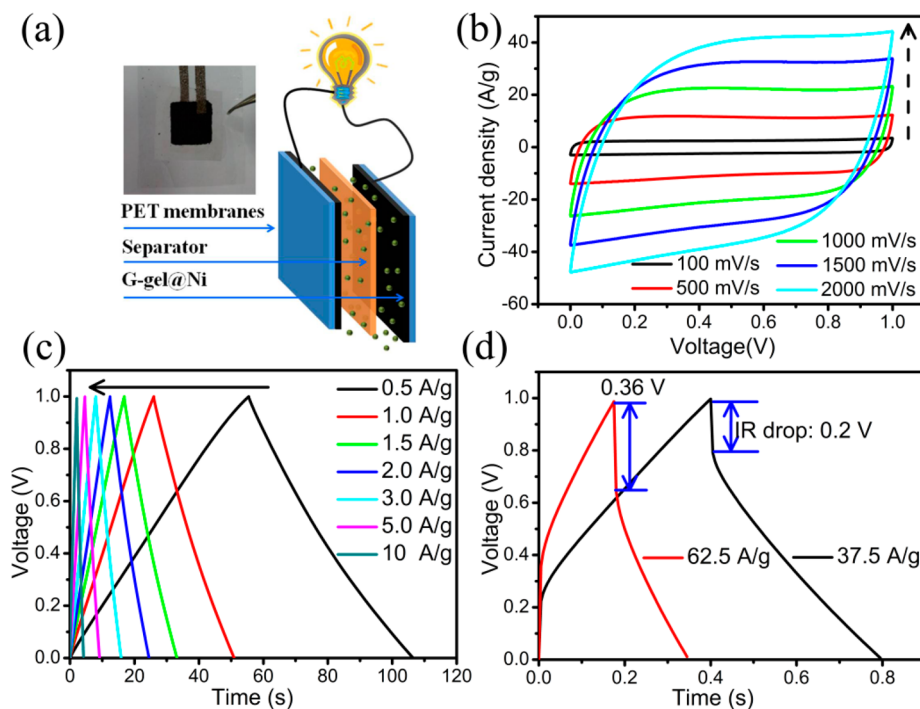
**Figure 6.** (a) Schematic of the structure of flexible supercapacitors consisting of two symmetrical rGO@Ni electrodes, a separator and two PET membranes, and the digital photographs of the flexible supercapacitor. (b) CV curves of rGO@Ni supercapacitor at different scan rates from 100 to 2000 mV/s. (c) GCD curves of rGO@Ni supercapacitor at different current densities from 0.5 to 10 A/g. (d) GCD curves at different current densities of 37.5 and 62.5 A/g.
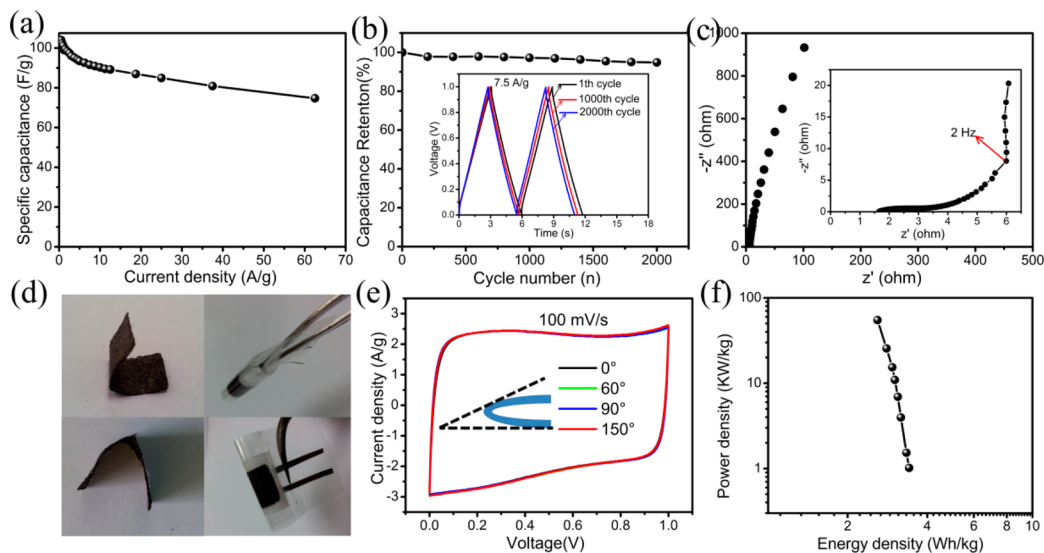


**Figure 7.** (a) Gravimetric specific capacitance of rGO@Ni supercapacitor at different current densities. (b) Cycle stability tests for rGO@Ni supercapacitor device at a current density of 7.5 A/g. Inset: GCD curve of the first, the 1000th, and the 2000th cycles for the device, respectively. (c) Nyquist plots of rGO@Ni supercapacitor. Inset: High-frequency region of the plots. (d) Photograph of the flexible supercapacitor device and bending rGO@Ni electrodes. (e) The CV curves of the flexible supercapacitor with bending angles of 0°, 60°, 90°, and 150° at a scan rate of 100 mV/s, respectively. (f) The Ragone plots of supercapacitor.

of nickel mass, but the ESR of the rGO foam with nickel all etched (attached Ti foil) was high up to 6.36 Ω. Considering the mass of the whole electrode, it is worth it for high gravimetric capacitance of the whole electrode to sacrifice some rate capability.

Furthermore, the mass loading per area of active material is also another important characteristic of the supercapacitors. The areal specific capacitance of rGO@Ni is easily modulated

by controlling the number of soaking to meet a variety of requirements in practical applications. The mass loading per area of rGO increases from 0.15 to 1.4 mg/cm$^2$ when the soak number is varied from 1 to 9 as shown in Figure 5a. Figure 5b and c clearly shows the area of CV curves at a scan rate of 100 mV/s and times of discharge increase at current density of 1 mA/cm$^2$ with increase of mass loading of rGO, and Figure 5d shows that the value of areal specific capacitance increases from

15.4 to 138.9 mF/cm$^2$ with the soak number varying from 1 to 9. These areal specific capacitance values are higher than those of the previously reported graphene such as laser-scribed graphene thin film (7.34 mF/cm$^2$),[33] graphene hydrogels deposited in nickel foams (41.6 mF/cm$^2$),[27] and graphene-cellulose paper (81 mF/cm$^2$).[43]

Because of the integration of graphene into the nickel conductive network, these rGO@Ni foams can be directly used to fabricate supercapacitor devices without additional of metal current collector and binder, which will increase the total mass of the electrode. The supercapacitor based on rGO@Ni electrode has exhibited good performance in high rate capability as shown in Figures 6 and 7. Figure 6a shows a schematic of the structure of supercapacitors device. A supercapacitor was assembled from two pieces of two rGO@Ni electrodes attached to PET membranes, each with 0.4 mg/cm$^2$ of rGO loading. The capacitive performance was evaluated by cyclic voltammograms (CV) and the galvanostatic charge−discharge (GCD) tests using 6 mol/L KOH aqueous solutions as electrolyte. The CV curves of flexible supercapacitor device at different scan rates ranging from 100 to 1000 mV/s are shown in Figure 6b. The CV curves exhibit typical quasi-rectangular shape, characteristic of the double-layer capacitor, indicating good charge propagations at the electrode interfaces following the mechanism of electric double-layer capacitors. Even at a high scan rate of 2000 mV/s, the CV curve of rGO@Ni is still close to rectangular, indicating a high rate capability and a low internal resistance.

The galvanostatic charge−discharge (GCD) curves of the rGO@Ni measured in a range of 0−1 V at different current densities from 0.5 to 62.5 A/g are shown in Figure 6c and d. The GCD curves look nearly symmetric; 0.2 and 0.36 V IR drop were observed at the beginning of discharge at high current densities of 37.5 and 62.5 A/g, respectively, also indicating our sample has good double-layer capacitive characteristics and low internal resistance. The specific capacitances of the rGO@Ni estimated from the discharging curves were ∼104, ∼101, ∼98, and ∼96 F/g at current densities of 0.5, 1, 2, and 3 A/g, respectively. These capacitance values are higher than or comparable to those of the 3D graphene foam such as graphene hydrogels deposited in nickel foams (120 F/g),[27] reduced graphene oxide foams by a leavening strategy (110 F/g),[29] graphene films grown on nickel foam by CVD (55.3 F/g),[44] graphene−Ni by CVD (25 F/g),[45] and graphene-gel/nickel foam by hydrothermal reaction (72.8 F/g),[46] but our approach has more simple and easy accessibility. If the total mass of electrodes is taken into consideration, our result is better than that of other 3D graphene on Ni foam.[27,28,47]

The gravimetric specific capacitance values at different current densities from 0.5 to 62.5 A/g are shown in Figure 7a. More importantly, at a high rate of 62.5 A/g, the rGO@Ni maintained 71% retention of its initial specific capacitance measured at 0.5 A/g (Figure 7a). The cycle stability is an important requirement for supercapacitor applications and was evaluated by repeating the GCD test at a current density of 7.5 A/g as shown in Figure 7b. The capacitance retention of rGO@Ni reaches ∼95% after 2000 cycles, and GCD curves of the 1000th and 2000th cycles inserted in Figure 7b maintain nearly symmetric the same as that of the first cycle, revealing an excellent cycle stability performance. These results indicate rGO@Ni has a high rate capacitive performance and excellent cycle stability, mainly due to the existence of 3D graphene/Ni

composite network structure and high electronic conductivity of graphene that can facilitate the efficient access of electrolyte ions to the graphene surface and shorten the ion diffusion path. The result is also supported by the electrochemical impedance spectroscopy (EIS) measured at open-circuit potential. The Nyquist plot based on a frequency response analysis of frequencies ranging from 0.01 Hz to 100 kHz with a 5 mV ac amplitude in 6 M KOH is shown in Figure 7c. At low frequencies, the straight line is nearly perpendicular to the real axis, while frequencies up to 2 Hz show excellent capacitive behavior. At high frequency (close to 100 kHz), the equivalent series resistance (ESR) obtained from the first intersection with the real axis is 1.68 Ω for rGO@Ni, indicating a low internal resistance for the whole device. These results revealed that this strategy of integrating graphene into the current collector as a whole electrode can improve the performance of rGO foam with the aid of a conductive network composed of a small amount of nickel.

Furthermore, the rGO@Ni supercapacitor device exhibits highly flexible and excellent mechanical robustness in the bending test. The CV curves obtained at the 100 mV/s scan rate with various bending angles are shown in Figure 7e. There are no significant differences between the CV curves with and without bending, suggesting the high flexible property for the rGO@Ni electrode. It is very meaningful for supercapacitors in the practical application. The relationship of power density ($P$) and energy densities ($E$) (Ragone plot) of the flexible supercapacitor device is shown in Figure 7f. The supercapacitor exhibits an energy density of 3.4 Wh/kg at a power density of 1.02 kW/kg in a 1 V window voltage at a current density of 2 A/g. It also preserves 76.5% of its energy density with a value of 2.6 Wh/kg as the power density increases to 54.9 kW/kg at a current density of 62.5 A/g. The existence of 3D architecture and conductive network composed of a small amount of nickel could improve the conductivity of chemical reduction graphene, resulting in a high rate capability, good cycle stability, low internal resistance, and excellent flexible properties; therefore, rGO@Ni electrode can replace graphene foam grown by CVD as an ideal platform to build graphene-based composites with other electrode materials for supercapacitor applications considering the cost and complexity of electrode preparation.

## 4. CONCLUSION

In summary, the graphene foam and 3D lightweight nickel network have been integrated together in depth without any polymeric binder and conductive additive by a simple strategy using commercial nickel foam as 3D substrate template. The nickel network and graphene composite foam have a continuous and interconnected 3D network structure similar to that of Ni foam. The flexible supercapacitor based on 3D Ni network and graphene composite foam has been studied for supercapacitor applications in detail, and it exhibited remarkable electrochemical performance including high rate capability performance, low contact resistance, excellent flexible properties, and a good adjustability of the areal specific capacitance. Such strategy effectively reduces the total mass of electrode and the contact resistance between rGO foam and the current collector. What is more important is that it provides a simple and highly versatile way to improve the performance of supercapacitors, and furthermore can integrate metal oxides, metal hydroxide, and conducting polymers into rGO@Ni composite electrode to enhance the gravimetric specific capacitance.

## ■ ASSOCIATED CONTENT

**⑤ Supporting Information**

Digital photograph of the nickel conductive network measurement by multimeter, Raman plot of rGO@Ni, table on the correlation of both the mass of residual nickel and the nickel conductive network, cyclic voltammetry (CV) curves, galvanostatic charge−discharge (GCD) curves, plots of gravimetric specific capacitance at different current densities on the influence of Ni support mass, and EIS plots of different Ni mass loading. This material is available free of charge via the Internet at http://pubs.acs.org.

## ■ AUTHOR INFORMATION

**Corresponding Author**

*E-mail: tangsl@nju.edu.cn.

**Notes**

The authors declare no competing financial interest.

## ■ ACKNOWLEDGMENTS

## ■ REFERENCES

(1) Miller, J. R.; Simon, P. Electrochemical Capacitors for Energy Management. *Science* **2008**, *321*, 651−652.

(2) Simon, P.; Gogotsi, Y. Materials for Electrochemical Capacitors. *Nat. Mater.* **2008**, *7*, 845−854.

(3) Wang, G.; Zhang, L.; Zhang, J. A Review of Electrode Materials for Electrochemical Supercapacitors. *Chem. Soc. Rev.* **2012**, *41*, 797−828.

(4) Miller, J. R.; Burke, A. F. Electrochemical Capacitors: Challenges and Opportunities for Real-world Applications. *Electrochem. Soc. Interface* **2008**, *17*, 53−57.

(5) Wei, H.; Ding, D.; Yan, X.; Guo, J.; Shao, L.; Chen, H.; Sun, L.; Colorado, H. A.; Wei, S.; Guo, Z. Tungsten Trioxide/Zinc Tungstate Bilayers: Electrochromic Behaviors, Energy Storage and Electron Transfer. *Electrochim. Acta* **2014**, *132*, 58−66.

(6) Wei, H.; Gu, H.; Guo, J.; Wei, S.; Liu, J.; Guo, Z. Silica Doped Nanopolyaniline with Endured Electrochemical Energy Storage and the Magnetic Field Effects. *J. Phys. Chem. C* **2013**, *117*, 13000−13010.

(7) Wei, H.; Zhu, J.; Wu, S.; Wei, S.; Guo, Z. Electrochromic Polyaniline/graphite Oxide Nanocomposites with Endured Electrochemical Energy Storage. *Polymer* **2013**, *54*, 1820−1831.

(8) Wei, H.; Gu, H.; Guo, J.; Wei, S.; Guo, Z. Electropolymerized Polyaniline Nanocomposites from Multi-Walled Carbon Nanotubes with Tuned Surface Functionalities for Electrochemical Energy Storage. *J. Electrochem. Soc.* **2013**, *160*, G3038−G3045.

(9) Wei, H.; Yan, X.; Wu, S.; Luo, Z.; Wei, S.; Guo, Z. Electropolymerized Polyaniline Stabilized Tungsten Oxide Nanocomposite Films: Electrochromic Behavior and Electrochemical Energy Storage. *J. Phys. Chem. C* **2012**, *116*, 25052−25064.

(10) Zhu, J.; Chen, M.; Qu, H.; Zhang, X.; Wei, H.; Luo, Z.; Colorado, H. A.; Wei, S.; Guo, Z. Interfacial Polymerized Polyaniline/graphite Oxide Nanocomposites Toward Electrochemical Energy Storage. *Polymer* **2012**, *53*, 5953−5964.

(11) Kuila, T.; Mishra, A. K.; Khanra, P.; Kim, N. H.; Lee, J. H. Recent Advances in The Efficient Reduction of Graphene Oxide and Its Application as Energy Storage Electrode Material. *Nanoscale* **2013**, *5*, 52−71.

(12) Li, C.; Shi, G. Three-dimensional Graphene Architectures. *Nanoscale* **2012**, *4*, 5549−5563.

(13) Sun, Y.; Wu, Q.; Shi, G. Graphene Based New Energy Materials. *Energy Environ. Sci.* **2011**, *4*, 1113−1132.

(14) Weiss, N. O.; Zhou, H.; Liao, L.; Liu, Y.; Jiang, S.; Huang, Y.; Duan, X. Graphene: An Emerging Electronic Material. *Adv. Mater.* **2012**, *24*, 5782−5825.

(15) Huang, Y.; Liang, J.; Chen, Y. An Overview of the Applications of Graphene-Based Materials in Supercapacitors. *Small* **2012**, *8*, 1805−1834.

(16) Yang, X.; Cheng, C.; Wang, Y.; Qiu, L.; Li, D. Liquid-Mediated Dense Integration of Graphene Materials for Compact Capacitive Energy Storage. *Science* **2013**, *341*, 534−537.

(17) Wassei, J. K.; Kaner, R. B. Oh, the Places You'll Go with Graphene. *Acc. Chem. Res.* **2013**, *46*, 2244−2253.

(18) Stoller, M. D.; Park, S.; Zhu, Y.; An, J.; Ruoff, R. S. Graphene-Based Ultracapacitors. *Nano Lett.* **2008**, *8*, 3498−3502.

(19) Stankovich, S.; Dikin, D. A.; Piner, R. D.; Kohlhaas, K. A.; Kleinhammes, A.; Jia, Y.; Wu, Y.; Nguyen, S. T.; Ruoff, R. S. Synthesis of Graphene-based Nanosheets via Chemical Reduction of Exfoliated Graphite Oxide. *Carbon* **2007**, *45*, 1558−1565.

(20) Worsley, M. A.; Pauzauskie, P. J.; Olson, T. Y.; Biener, J.; Satcher, J. H., Jr.; Baumann, T. F. Synthesis of Graphene Aerogel with High Electrical Conductivity. *J. Am. Chem. Soc.* **2010**, *132*, 14067−14069.

(21) Xu, Y.; Lin, Z.; Huang, X.; Liu, Y.; Huang, Y.; Duan, X. Flexible Solid-State Supercapacitors Based on Three-Dimensional Graphene Hydrogel Films. *ACS Nano* **2013**, *7*, 4042−4049.

(22) Xu, Y.; Sheng, K.; Li, C.; Shi, G. Self-assembled Graphene Hydrogel via A One-step Hydrothermal Process. *ACS Nano* **2010**, *4*, 4324−4330.

(23) Yu, Q.; Lian, J.; Siriponglert, S.; Li, H.; Chen, Y. P.; Pei, S.-S. Graphene Segregated on Ni Surfaces and Transferred to Insulators. *Appl. Phys. Lett.* **2008**, *93*, 113103.

(24) Kim, K. S.; Zhao, Y.; Jang, H.; Lee, S. Y.; Kim, J. M.; Kim, K. S.; Ahn, J. H.; Kim, P.; Choi, J. Y.; Hong, B. H. Large-scale Pattern Growth of Graphene Films for Stretchable Transparent Electrodes. *Nature* **2009**, *457*, 706−710.

(25) Li, X.; Cai, W.; An, J.; Kim, S.; Nah, J.; Yang, D.; Piner, R.; Velamakanni, A.; Jung, I.; Tutuc, E.; Banerjee, S. K.; Colombo, L.; Ruoff, R. S. Large-area Synthesis of High-quality and Uniform Graphene Films on Copper Foils. *Science* **2009**, *324*, 1312−1314.

(26) Chen, Z.; Ren, W.; Gao, L.; Liu, B.; Pei, S.; Cheng, H.-M. Three-dimensional Flexible and Conductive Interconnected Graphene networks grown by Chemical VapourDeposition. *Nat. Mater.* **2011**, *10*, 424−428.

(27) Chen, J.; Sheng, K.; Luo, P.; Li, C.; Shi, G. Graphene Hydrogels Deposited in Nickel Foams for High-Rate Electrochemical Capacitors. *Adv. Mater.* **2012**, *24*, 4569−4573.

(28) Ye, S.; Feng, J.; Wu, P. Deposition of Three-Dimensional Graphene Aerogel on Nickel Foam as a Binder-Free Supercapacitor Electrode. *ACS Appl. Mater. Interfaces* **2013**, *5*, 7122−7129.

(29) Niu, Z.; Chen, J.; Hng, H. H.; Ma, J.; Chen, X. A Leavening Strategy to Prepare Reduced Graphene Oxide Foams. *Adv. Mater.* **2012**, *24*, 4144−4150.

(30) Choi, B. G.; Yang, M.; Hong, W. H.; Choi, J. W.; Huh, Y. S. 3D Macroporous Graphene Frameworks for Supercapacitors with High Energy and Power Densities. *ACS Nano* **2012**, *6*, 4020−4028.

(31) Lee, J. H.; Park, N.; Kim, B. G.; Jung, D. S.; Im, K.; Hur, J.; Choi, J. W. Restacking-Inhibited 3D Reduced Graphene Oxide for High Performance Supercapacitor Electrodes. *ACS Nano* **2013**, *7*, 9366−9374.

(32) Beidaghi, M.; Wang, C. Micro-Supercapacitors Based on Interdigital Electrodes of Reduced Graphene Oxide and Carbon Nanotube Composites with Ultrahigh Power Handling Performance. *Adv. Funct. Mater.* **2012**, *22*, 4501−4510.

(33) El-Kady, M. F.; Strong, V.; Dubin, S.; Kaner, R. B. Laser Scribing of High-Performance and Flexible Graphene-Based Electrochemical Capacitors. *Science* **2012**, *335*, 1326−1330.

(34) Ji, J.; Zhang, L. L.; Ji, H.; Li, Y.; Zhao, X.; Bai, X.; Fan, X.; Zhang, F.; Ruoff, R. S. Nanoporous Ni(OH)$_2$ Thin Film on 3D Ultrathin-Graphite Foam for Asymmetric Supercapacitor. *ACS Nano* **2013**, *7*, 6237−6243.

10256

dx.doi.org/10.1021/am501635h | *ACS Appl. Mater. Interfaces* 2014, 6, 10248−10257

(35) Gogotsi, Y.; Simon, P. True Performance Metrics in Electrochemical Energy Storage. *Science* **2011**, *334*, 917−918.

(36) Pei, S.; Zhao, J.; Du, J.; Ren, W.; Cheng, H.-M. Direct Reduction of Graphene Oxide Films into Highly Conductive and Flexible Graphene Films by Hydrohalic Acids. *Carbon* **2010**, *48*, 4466−4474.

(37) Prasai, D.; Tuberquia, J. C.; Harl, R. R.; Jennings, G. K.; Bolotin, K. I. G Graphene: Corrosion-Inhibiting Coating. *ACS Nano* **2012**, *6*, 1102−1108.

(38) Ji, H.; Zhang, L.; Pettes, M. T.; Li, H.; Chen, S.; Shi, L.; Piner, R.; Ruoff, R. S. Ultrathin Graphite Foam: A Three-Dimensional Conductive Network for Battery Electrodes. *Nano Lett.* **2012**, *12*, 2446−2451.

(39) Xu, Y.; Shi, G. Assembly of Chemically Modified Graphene: Methods and Applications. *J. Mater. Chem.* **2011**, *21*, 3311−3323.

(40) Huang, H.; Xu, L.; Tang, Y.; Tang, S.; Du, Y. Facile Synthesis of Nickel Network Supported Three-dimensional Graphene Gel as A Lightweight and Binder-free Electrode for High Rate Performance Supercapacitor Application. *Nanoscale* **2013**, 2426−2433.

(41) Stoller, M. D.; Ruoff, R. S. Best Practice Methods for Determining an Electrode Material's Performance for Ultracapacitors. *Energy Environ. Sci.* **2010**, *3*, 1294−1301.

(42) He, Y.; Chen, W.; Li, X.; Zhang, Z.; Fu, J.; Zhao, C.; Xie, E. Freestanding Three-Dimensional Graphene/$MnO_2$ Composite Networks As Ultralight and Flexible Supercapacitor Electrodes. *ACS Nano* **2012**, *7*, 174−182.

(43) Weng, Z.; Su, Y.; Wang, D.-W.; Li, F.; Du, J.; Cheng, H.-M. Graphene-Cellulose Paper Flexible Supercapacitors. *Adv. Energy Mater.* **2011**, *1*, 917−922.

(44) Chen, W.; Fan, Z.; Zeng, G.; Lai, Z. Layer-dependent Supercapacitance of Graphene Films Grown by Chemical Vapor Deposition on Nickel Foam. *J. Power Sources* **2013**, *225*, 251−256.

(45) Zhu, G.; He, Z.; Chen, J.; Zhao, J.; Feng, X.; Ma, Y.; Fan, Q.; Wang, L.; Huang, W. Highly Conductive Three-dimensional $MnO_2$-carbon Nanotube-graphene-Ni Hybrid Foam as a Binder-free Supercapacitor Electrode. *Nanoscale* **2014**, *6*, 1079−1085.

(46) Zhai, T.; Wang, F.; Yu, M.; Xie, S.; Liang, C.; Li, C.; Xiao, F.; Tang, R.; Wu, Q.; Lu, X.; Tong, Y. 3D $MnO_2$-graphene Composites with Large Areal Capacitance for High-Performance Asymmetric Supercapacitors. *Nanoscale* **2013**, *5*, 6790−6796.

(47) Huang, Z.; Zhang, H.; Chen, Y.; Wang, W.; Chen, Y.; Zhong, Y. Microwave-assisted Synthesis of Functionalized Graphene on Ni Foam as Electrodes for Supercapacitor Application. *Electrochim. Acta* **2013**, *108*, 421−428.